Harvesting Energy from Water Flow over Graphene

ARTICLE *in* NANO LETTERS · AUGUST 2011

Impact Factor: 13.59 · DOI: 10.1021/nl2011559 · Source: PubMed

7 AUTHORS, INCLUDING:

Prashant Dhiman
National Institute of Technology, Hamirpur
16 PUBLICATIONS **132** CITATIONS
SEE PROFILE

Fazel Yavari
Northwestern University
19 PUBLICATIONS **1,098** CITATIONS
SEE PROFILE

Hemtej Gullapalli
Rice University
16 PUBLICATIONS **1,127** CITATIONS
SEE PROFILE

Yunfeng Shi
Rensselaer Polytechnic Institute
65 PUBLICATIONS **1,183** CITATIONS
SEE PROFILE

NANO LETTERS

LETTER

pubs.acs.org/NanoLett

Harvesting Energy from Water Flow over Graphene

Prashant Dhiman,[†,∥] Fazel Yavari,[†,∥] Xi Mi,[‡] Hemtej Gullapalli,[§] Yunfeng Shi,[‡] Pulickel M. Ajayan,[§] and Nikhil Koratkar*[,†,‡]

[†]Department of Mechanical, Aerospace, and Nuclear Engineering, [‡]Department of Materials Science and Engineering, Rensselaer Polytechnic Institute, Troy, New York 12180, United States

[§]Department of Mechanical and Materials Engineering, Rice University, Houston, Texas, United States

Supporting Information

ABSTRACT: Water flow over carbon nanotubes has been shown to generate an induced voltage in the flow direction due to coupling of ions present in water with free charge carriers in the nanotubes. However, the induced voltages are typically of the order of a few millivolts, too small for significant power generation. Here we perform tests involving water flow with various molarities of hydrochloric acid (HCl) over few-layered graphene and report order of magnitude higher induced voltages for graphene as compared to nanotubes. The power generated by the flow of ~0.6 M HCl solution at ~0.01 m/sec was measured to be ~85 nW for a ~30 × 16 μm size graphene film, which equates to a power per unit area of ~175 W/m^2. Molecular dynamics simulations indicate that the power generation is primarily caused by a net drift velocity of adsorbed Cl^- ions on the continuous graphene film surface.

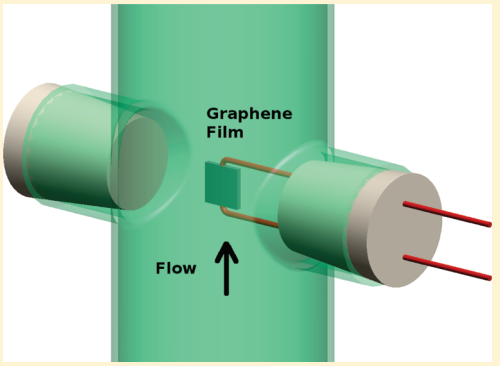

KEYWORDS: Graphene, energy harvesting, water flow, surface ion hopping

Over the past decade a number of theoretical[1−3] and experimental studies[4−7] have demonstrated that flow of water or other polar liquids over one-dimensional structures such as carbon nanotubes generates a net potential difference and associated electric current in the nanotubes along the flow direction. A number of mechanisms such as phonon drag (transfer of momentum from the flowing liquid to the acoustic phonons in the nanotube, which in turn drags free charge carriers in the nanotube),[1] surface ion hopping,[3] direct scattering of the free charge carriers from the fluctuating Coulombic fields of the ions in the flowing liquid,[1] fluctuating asymmetric potential,[4] and streaming potential models[2] have been proposed to explain this effect. However, a common observation from the experimental studies[4−7] with carbon nanotubes is that the induced voltages generated by water flow are <10 mV. While a few millivolts signal is sufficient for miniaturized flow sensor type application, it is not enough for harvesting significant amounts of energy from the flow environment. Here, we report the results of flow transport experiments over few-layered graphene films and observe an order of magnitude increase in induced voltage for graphene compared to carbon nanotubes. The current and power output of the graphene device was also measured by connecting an external resistor (load) across the graphene film. Using a ~30 × 16 μm size graphene film, we generated ~85 nW of power at a flow velocity of ~0.01 m/sec, which translates to a specific power output of ~175 W/m^2. Molecular dynamics simulations for Cl^- ion drift velocity on a graphene sheet as a function of the bulk flow velocity showed qualitative agreement with experimental observations for the induced voltage response. This indicates that coupling of the free charges that are present in graphene with the mobile surface charges (i.e., adsorbed ions) is the main mechanism responsible for power generation from the flow.

Graphene samples were synthesized by chemical vapor deposition (CVD) on copper (Cu) foil using liquid precursor hexane.[8,9] After growth, a thin poly(methyl methacrylate) (PMMA) film was coated on the graphene/Cu substrate. The underlying Cu substrate was dissolved in dilute HNO_3, and the film was transferred onto a Si substrate with ~300 nm thick insulating SiO_2 layer. Photolithography followed with e-beam evaporator deposition was used to pattern four electrodes (Ti/Au, 3/30 nm) on the top surface of the transferred graphene film. The optical micrograph in Figure 1a shows the graphene film with the electrodes deposited on the top surface. The scanning electron micrograph in Figure 1b indicates that the region of the graphene film that is enclosed within the electrode pattern is ~30 μm × 16 μm. Raman spectroscopy using 514 nm wavelength excitation gave the G band (~1581 cm^{-1}) and 2D band (2669 cm^{-1}) peaks that are characteristic of graphene (Supporting Information Figure S1). The strongly suppressed D band indicates high quality (defect-free) graphene grown by our CVD method. The intensity ratio of the G and 2D modes was ~0.5, which indicates a few-layered graphene sample.[10,11] This was also confirmed by atomic force microscopy characterization of the graphene film (Supporting Information, Figure S2). Using gold wires and silver epoxy (EJ-2189 two part kit from EPOXY Technology), the contact pads shown in Figure 1a were

Received: April 6, 2011
Revised: June 28, 2011

   dx.doi.org/10.1021/nl2011559 | *Nano Lett.* XXXX, XXX, 000–000

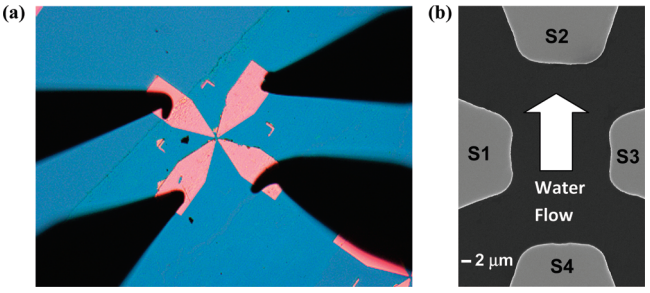

Figure 1. (a) Optical micrograph of a typical graphene film on an Si/SiO_2 substrate with contact electrodes. (b) Scanning electron micrograph of the graphene film within the electrode pattern showing film lateral dimensions of ~30 μm × 16 μm. The electrodes are numbered S1−S4; only two electrodes (S2, S4) are used to measure the flow induced voltages and currents. Arrow indicates the flow direction.

connected to the leads of a conventional chip carrier making it possible to electrically address the graphene film. In addition to the graphene, a film comprised of aligned multwalled carbon nanotubes (MWNT) was also tested. The MWNT diameter was ~10 nm and length was ~1 mm. Transmission and scanning electron microscopy imaging of the aligned MWNT are shown in the Supporting Information (Figures S3 and S4). The chemical vapor deposition method that was used for MWNT fabrication is also described in the Supporting Information.

The schematic layout of the flow test facility is depicted in Figure 2a. The closed-loop system consists of an overhead tank that stores the water. Gravity forces the water down toward the test section of the tunnel. The rate of fluid flow is accurately controlled using flow control valves. The test section consists of a long hollow tube with dimensions designed to minimize turbulence and boundary layer interference in the center of the test section where the samples are mounted. The graphene film is mounted parallel with the flow direction (inset in Figure 2a). The fluid is collected in a sump-tank and then pumped back up to the overhead tank to complete the loop. All tests are performed at room temperature (~70 °F). The induced voltage and current responses are measured in real-time using a Labview-based data acquisition system. The flow speed in the test section is estimated based on the mass flow rate controlled by the valves and the known cross-sectional area of the test section.

Typical results for the induced voltage measured across terminals (S2−S4) for fluid flow along the direction S2−S4 (see Figure 1b) is shown in Figure 2b. Note that there was no significant flow dependent voltage generated between terminals S1 and S3. In addition to graphene, aligned multiwalled carbon nanotubes (MWNT, ~1 mm in length[12]) were also tested with water flow aligned along the main axis of the nanotube. The fluid used was deionized water with various concentrations of hydrochloric acid (HCl, 0 to 0.6 M). The induced voltage showed a strong sensitivity to the HCl content (Figure 2b). For instance at ~0.6 M HCl, a peak induced voltage of ~30 mV was generated, which dropped to ~8 mV at ~0.3 M HCl. These values are over 1 order of magnitude higher than the result for the carbon nanotube film (~0.8 mV) at ~0.6 M HCl concentration. Above 0.6 M concentration there was no significant increase in the induced voltages. For deionized (DI) water, the induced voltages generated were of the order of a few microvolts for both the MWNT and graphene samples. The results were reproducible for over five different graphene film samples that we tested (mean and standard deviation values are provided in the Supporting Information). Note that there is always a small DC voltage (Supporting Information) generated when the sample is dipped in the ionic fluid resulting from electrode mismatch or chemical doping effects. In all the plots shown in Figure 2b, this DC voltage was subtracted out to reveal the flow-induced voltage generation effect. In order to determine whether the graphene region outside of the electrode contacts significantly influences the measurements made within the electrode region, we contacted a small fragment of graphene (Supporting Information Figure S5) and repeated the experiments at ~0.6 M HCl concentration. The flow-induced voltages created on this sample are compared in Figure S6 (Supporting Information) to the results shown in Figure 2b for the large area graphene film. Both samples generate nearly the same induced voltages, indicating that the measured voltage is mainly influenced by the electrode defined area.

Another very interesting feature of the testing was that we observed a saturation effect wherein the induced voltage increases with the induced flow speed and then levels out or saturates at a certain level. This nonlinear dependence of the induced voltage on the bulk flow velocity was consistent for five separate films that we tested and was observed independent of the molarity of the HCl solution. We also measured the power generation in our graphene film for ~0.6 M HCl solution at a flow velocity of ~0.01 m/sec. For this, an external load (resistor, R) was connected in the circuit and the flow-induced current (I) was measured. Figure 3a shows the power (I^2R) produced for different external loads in the circuit. The corresponding flow-induced current (I) versus flow-induced voltage (V) curve generated by ~0.01 m/sec flow of 0.6 M HCl solution over the graphene sample is shown in the Supporting Information (Figure S7). When the resistance is zero, the circuit is short-circuited and the power drops to zero. The other extreme is when the resistance is infinite for which case the circuit is open-loop and again the power drops to zero. The optimal power output is attained when the external load matches the internal impedance of the film. For our system this optimal resistance is ~5 kΩ. The power output for this case exceeds ~85 nW, which is impressive considering the relatively small lateral dimensions (~30 × 16 μm) of the graphene film that was tested. This level of power generation is sufficient to charge a capacitor that can be utilized to intermittently power microsensor devices deployed remotely in the field. For ~0.6 M HCl solution flowing at a velocity of ~0.01 m/sec, the specific power (i.e., power produced per unit area) generated by the graphene device is ~175 W/m^2, which indicates the potential for significantly higher levels of absolute power generation if the size of the graphene film can be scaled up. Recent advances in the CVD growth of graphene on large area substrates makes this a possibility.[13−15] The specific power of our device compares well with recently reported nanoengineered battery concepts[16] that extract energy from a water salinity difference and have been reported to generate power densities of ~0.138 W/m^2

To gain insight into the mechanism(s) responsible for power generation in our graphene films, we performed molecular dynamics (MD) simulations of the interaction of HCl solution and the graphene surface. The simulation cell consisted of two parallel single-layered graphene planes with water molecules, Cl^- ions and H_3O^+ ions sandwiched in-between (inset in Figure 3b). The simulation box is 42.6 Å × 24.6 Å × 100 Å in size with periodic boundary conditions, and consists of 800 carbon atoms

dx.doi.org/10.1021/nl2011559 |*Nano Lett.* XXXX, XXX, 000–000

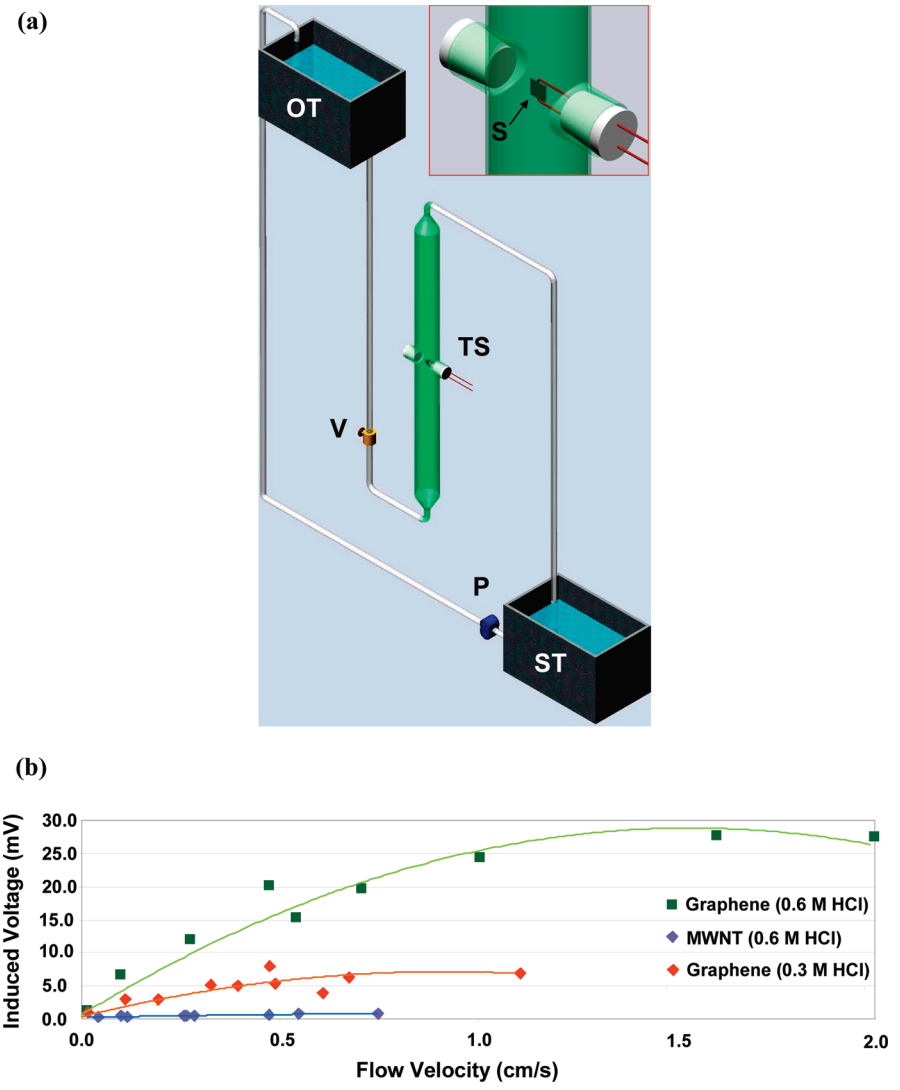

Figure 2. (a) Schematic illustration of the water tunnel used to perform the flow transport experiments. OT, overhead tank; ST, sump tank; TS, test section; V, flow control valve; P, pump; and S, sample to be tested. In the experiments the fluid flow is aligned parallel to the graphene film as indicated in the inset schematic. (b) Induced voltage as a function of fluid flow velocity for the graphene film (exposed to ~0.6 and ~0.3 M HCl solutions) and for a multiwalled carbon nanotube (MWNT) film exposed to a ~0.6 M HCl solution.

and 1000 water molecules. The graphene planes lie in $x-y$ plane and separated by 35 Å in z direction to maintain atmospheric pressure. Under the above conditions, the water achieves a density of 1.0 g/cm^3 at room temperature. The number density of H_3O^+ and Cl^- ions are set to be ~0.6 M, which is also used in the experiments. A flexible simple point-charge (SPC) model[17] is used to describe water molecules. This model uses harmonic force fields to constrain O−H bonds to be 1.0 Å and H−O−H angles to be 109.47°. H and O atoms are charged with 0.41 and −0.82 e, Cl atoms are charged with −1.0 e. H_3O^+ ions are described by the same constraints for O−H bonds and H−O−H angles as those used for water molecules. The O and H atoms in hydronium ions are charged with −0.554 and 0.518 e, respectively,[18] resulting in +1.0 e charge for each H_3O^+. Such treatment is appropriate[18,19] where proton transfer is not considered. The graphene sheets are described by molecular mechanics force field AMBER[20] and are kept charge neutral. Pairwise Lennard-Jones (LJ) potential is used for O−O[21] and C−O[22] (for both H_2O and H_3O^+) interactions. Interactions between graphene and Cl^- are described by LJ force field parametrized by ab initio calculations.[23,24] The interactions between ions are Coulombic with short-range repulsion forces implemented for each type of atoms to prevent atoms from overlapping. A bulk flow velocity is imparted to the fluid as follows. A thin water slab (~2 Å) in the middle of the water region is assigned a constant velocity. Graphene planes are flexible but their centers of mass are fixed to prevent the graphene from shifting. The entire system evolves under NVT (canonical) ensemble at 298 K for 800 ps with an integration step of 1 fs. Because of significant thermal fluctuation (most probable molecular velocity from Maxwell distribution is 525 m/s at 298 K), the flow speeds in the simulations were chosen to be quite large (about 1−20 m/s, much faster than in the experiments ~0.01 m/s) in order to overcome the significant thermal noise within reasonable computational time.

Adsorption, desorption, and hopping of Cl^- ions were observed on the flexible graphene sheets. However, hydronium ions flow with water without adsorbing or hopping on graphene

dx.doi.org/10.1021/nl2011559 |*Nano Lett.* XXXX, XXX, 000–000

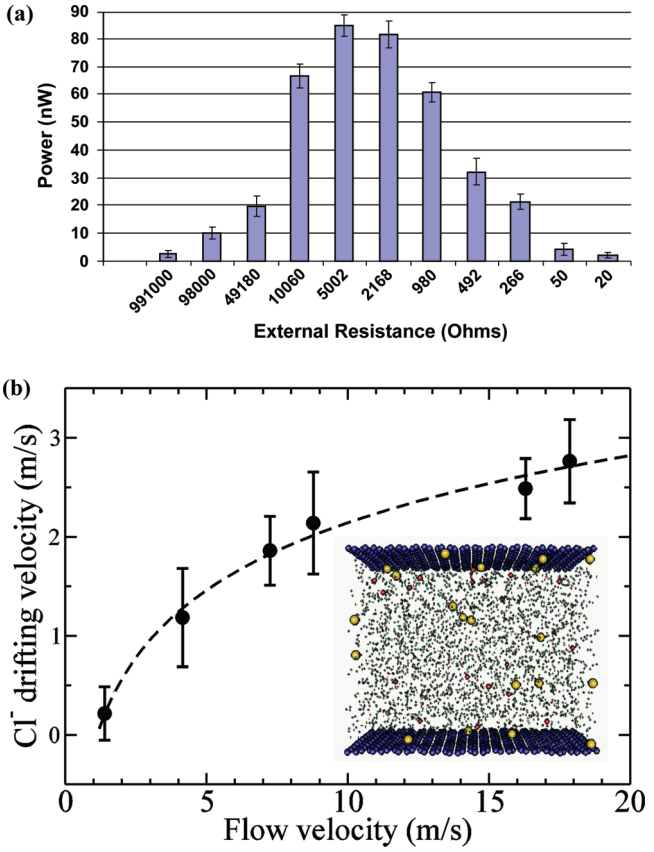

Figure 3. (a) Power generated by graphene film at a flow speed of ~0.01 m/sec for 0.6 M HCl solution. Power output is shown as a function of the external resistor (load) connected to the device. The maximum power harvested from the flow by the graphene films is ~85 nW for ~5 kΩ resistive load in the circuit. (b) Molecular dynamics simulations of Cl^- ion drift velocity on the surface of a graphene sheet as a function of the bulk flow velocity. The error bar is the fitting error associated with linear fitting of the accumulated displacement vs simulation time. The ion drift speed is observed to saturate with increasing flow speed consistent with the experimental observations. Inset shows the simulation cell comprised of two parallel single-layered graphene planes with water molecules (small dots), H_3O^+ (red spheres), and Cl^- ions (yellow spheres) sandwiched in-between.

sheets, which is due to their weaker interactions with the graphene. Most interestingly we observe a sublinear hopping speed as a function of flow velocity as indicated in Figure 3b. In fact, as the bulk flow velocity is increased the ion hopping drift velocity saturates just as the induced voltages were observed to saturate (Figure 2b) in the experiments. Note that the MD model qualitatively captures the drift of the adsorbed ions on the graphene surface but cannot be used as a quantitative measure since the time and length scales involved in the simulations are very different from the experiments. The drift of the adsorbed surface ions arises from stick−slip motion due to friction between the surface layer and the bulk flow. Many such systems (ref 3) exhibiting stick−slip motion such as charge density wave, flux-line systems, or atomic force microscope tips moving in a pinning potential show a linear relation between the driving force and the logarithm of the velocity. So if the velocity is plotted on a linear scale (as in Figure 2b), there will appear to be a near saturation effect at high velocities. This saturation effect is expected to not change with the sample size or ionic content.

On the basis of the MD simulation results and the experimental observations that show a similar saturation effect, it appears that surface ion hopping[3] is the main mechanism responsible for power generation in our system. Phonon dragging[1] and streaming potential models[2] are unlikely since they predict linear increase in the induced voltage with the flow velocity, while we observe a nonlinear response. Direct scattering of the free carriers from the fluctuating Coulombic fields of the ions is shown to be a relatively weak effect.[1] The fluctuating asymmetric potential model[4] needs to invoke pulsating asymmetric ratchets for which there is no direct evidence. Our MD simulations show evidence of physical drift of adsorbed Cl^- ions which leads us to the explanation that we propose. Essentially, the ions in the flow acquire a certain net drift velocity on the surface of the graphene sheets in the direction of the flow. This originates from continuous adsorption and desorption (i.e., stick−slip) motion of the surface ions. Because of the nanometer scale thickness of the sheets, these surface ions couple with free-charge carriers in the graphene sheets. The net result is that the free charges are dragged in the flow direction resulting in an induced current and induced voltage in the flow direction. We used this model to obtain a ball-park estimate of the induced voltages for our graphene films. Assuming a surface ion drift velocity (v) of ~0.01 m/sec (upper limit at the point of saturation), film length (L) ~30 μm, graphene sheet resistance (R) of ~5 kΩ, electronic charge (e) of 1.6×10^{-19} C, an upper limit[25] of the charge carrier density (σ) in graphene to be in the range of ~10^{19} −10^{20} m^{-2}, the induced voltage ($V = RI$, $I = \sigma eLv$) equates to ~2.5−25 mV, which is in the range of what we have measured experimentally. Note that our choice of HCl was based on the fact that only Cl^- ions are involved in surface hopping and not the hydronium (H_3O^+) ions. If one were to use NaCl instead then it is likely that adsorbed Na^+ ions present on the graphene would also be dragged along the flow direction and this would create a current in the graphene in the opposite direction that would cancel out or reduce the current flow resulting from the Cl^- ion drift. By contrast, for H^+ this is not an issue because they combine with water molecules to form stable hydronium ions. Our simulations indicate that hydronium ions flow with water without adsorbing or hopping on graphene sheets, which is due to their weaker interactions with the graphene.

There are several reasons why power generation from water flow over graphene is superior to carbon nanotubes. (1) In a bulk singlewalled carbon nanotube sample (as in ref 4), only one-third of the nanotubes are metallic and the rest are semiconducting. As a result, the available charge carrier density is suppressed for such a singlewalled carbon nanotube film as compared to graphene, which behaves as a semimetal with exceptionally high electron mobilities.[26,27] (2) Interfaces in carbon nanotube networks are lossy.[28] This impedes electron-hopping across the interfaces and reduces the magnitude of the current and voltages that are induced by the fluid flow. By contrast, the graphene film is a continuous sheet that spans the entire gap between the electrodes. There are no breaks in the film, which entirely eliminates all sheet-to-sheet interfaces in graphene giving it a huge advantage compared to a network of carbon nanotubes. (3) Ion transport in a nanotube bundle or a nanotube rope is complicated and there are several effects such as entrance effects, interface effects, tube-to-tube hopping constraints, etc., which may serve to limit the effectiveness of ion hopping in the case of a nanotube network.[29,30] By contrast, the graphene films that we tested are flat sheets and surface ions can efficiently glide or drift on the

dx.doi.org/10.1021/nl2011559 |*Nano Lett.* XXXX, XXX, 000–000

surface leading to higher induced voltages and currents with an associated increase in the power generation performance.

■ ASSOCIATED CONTENT

Supporting Information. Raman spectroscopy study of the graphene film sample. Flow-induced current (I) versus flow-induced voltage (V) response for the graphene sample for flow of ~0.6 M HCl solution at a speed of ~0.01 m/sec. Experiments to study the effect of the graphene region outside of the electrical contacts on the flow induced voltages. Scanning and transmission electron microscopy characterization of the multiwalled carbon nanotube film. Atomic force microscopy characterization of the graphene film. Voltage at zero flow speed and induced voltages generated at various flow speeds and HCl ion concentrations presented in tabular form. This material is available free of charge via the Internet at http://pubs.acs.org.

■ AUTHOR INFORMATION

Corresponding Author
*E-mail: koratn@rpi.edu.

Author Contributions
‖These authors contributed equally to this work.

■ ACKNOWLEDGMENT

N.K., P.M.A. and Y.S. acknowledge funding support for this research from the Advanced Energy Consortium (AEC).

■ REFERENCES

(1) Kral, P.; Shapiro, M. *Phys. Rev. Lett.* **2001**, *86*, 131–134.
(2) Cohen, A. E. *Science* **2003**, *300*, 1235–1235.
(3) Persson, B. N. J.; Tartaglino, U.; Tosatti, E.; Ueba, H. *Phys. Rev. B* **2004**, *69*, 235410.
(4) Ghosh, S.; Sood, A. K.; Kumar, N. *Science* **2003**, *299*, 1042–1044.
(5) Ghosh, S.; Sood, A. K.; Ramaswamy, S.; Kumar, N. *Phys. Rev. B* **2004**, *70*, 205423.
(6) Liu, Z.; Zheng, K. H.; Hu, L. J.; Liu, J.; Qiu, C. Y.; Zhou, H. Q.; Huang, H. B.; Yang, H. F.; Li, M.; Gu, C. Z.; Xie, S. S.; Qiao, L. J.; Sun, L. F. *Adv. Mater.* **2010**, *22*, 999–1003.
(7) Zhao, Y. C.; Song, L.; Deng, K.; Liu, Z.; Zhang, Z. X.; Yang, Y. L.; Wang, C.; Yang, H. F.; Jin, A. Z.; Luo, Q.; Gu, C. Z.; Xie, S. S.; Sun, L. F. *Adv. Mater.* **2008**, *20*, 1772–1776.
(8) Srivastava, A.; Galande, C.; Ci, L.; Song, L.; Rai, C.; Jariwala, D.; Kelly, K. F.; Ajayan, P. M. *Chem. Mater.* **2010**, *22*, 3457–3461.
(9) Yavari, F.; Kritzinger, C.; Gaire, C.; Song, L.; Gullapalli, H.; Borca-Tasciuc, T.; Ajayan, P. M.; Koratkar, N. *Small* **2010**, *6*, 2535–2538.
(10) Graf, D.; Molitor, F.; Ensslin, K.; Stampfer, C.; Jungen, A.; Hierold, C.; Wirtz, L. *Nano Lett.* **2007**, *7*, 238–242.
(11) Gupta, A.; Chen, G.; Joshi, P.; Tadigadapa, S.; Eklund, P. C. *Nano Lett.* **2006**, *6*, 2667–2673.
(12) Wang, Z. K.; Ci, L. J.; Chen, L.; Nayak, S.; Ajayan, P. M.; Koratkar, N. *Nano Lett.* **2007**, *7*, 697–702.
(13) Bae, S.; Kim, H.; Lee, Y.; Xu, X. F.; Park, J. S.; Zheng, Y.; Balakrishnan, J.; Lei, T.; Kim, H. R.; Song, Y. I.; Kim, Y. J.; Kim, K. S.; Ozyilmaz, B.; Ahn, J. H.; Hong, B. H.; Iijima, S. *Nat. Nanotechnol.* **2010**, *5*, 574–578.
(14) Kim, K. S.; Zhao, Y.; Jang, H.; Lee, S. Y.; Kim, J. M.; Ahn, J. H.; Kim, P.; Choi, J. Y.; Hong, B. H. *Nature* **2009**, *457*, 706–710.
(15) Li, X. S.; Cai, W. W.; An, J. H.; Kim, S.; Nah, J.; Yang, D. X.; Piner, R.; Velamakanni, A.; Jung, I.; Tutuc, E.; Banerjee, S. K.; Colombo, L.; Ruoff, R. S. *Science* **2009**, *324*, 1312–1314.
(16) La Mantia, F.; Pasta, M.; Deshazer, H. D.; Logan, B. E.; Cui, Y. *Nano Lett.* **2011**, *11*, 1810–1813.
(17) Zhu, S. B.; Fillingim, T. G.; Robinson, G. W. *J. Phys. Chem.* **1991**, *95*, 1002–1006.
(18) Urata, S.; Irisawa, J.; Takada, A.; Shinoda, W.; Tsuzuki, S.; Mikami, M. *J. Phy. Chem. B* **2005**, *109*, 4269–4278.
(19) Cui, S.; Liu, J.; Selvan, M. E.; Keffer, D. J.; Edwards, B. J.; Steele, W. V. *J. Phys. Chem. B* **2007**, *111*, 2208–2218.
(20) Cornell, W. D.; Cieplak, P.; Bayly, C. I.; Gould, I. R.; Merz, K. M.; Ferguson, D. M.; Spellmeyer, D. C.; Fox, T.; Caldwell, J. W.; Kollman, P. A. *J. Am. Chem. Soc.* **1995**, *117*, 5179–5197.
(21) Toukan, K.; Rahman, A. *Phys. Rev. B* **1985**, *31*, 2643.
(22) Werder, T.; Walther, J. H.; Jaffe, R. L.; Halicioglu, T.; Koumoutsakos, P. *J. Phys. Chem. B* **2003**, *107*, 1345–1352.
(23) Medeiros, P. V. C.; Mascarenhas, A. J. S.; de Brito Mota, F.; de Castilho, C. M. C. *Nanotechnology* **2010**, *21*, 485701.
(24) Hummer, G.; Rasaiah, J. C.; Noworyta, J. P. *Nature* **2001**, *414*, 188–190.
(25) Fang, T.; Konar, A.; Xing, H.; Jena, D. *Appl. Phys. Lett.* **2007**, *91*, 092109.
(26) Park, S.; Ruoff, R. S. *Nat. Nanotechnol.* **2009**, *4*, 217–224.
(27) Geim, A. K.; Novoselov, K. S. *Nat. Mater.* **2007**, *6*, 183–191.
(28) Amama, P. B.; Lan, C.; Cola, B. A.; Xu, X.; Reifenberger, R. G.; Fisher, T. S. *J. Phys. Chem. C* **2008**, *112*, 19727–19733.
(29) Mukherjee, B.; Maiti, P. K.; Dasgupta, C.; Sood, A. K. *ACS Nano* **2008**, *2*, 1189–1196.
(30) Mao, Z. G.; Sinnott, S. B. *J. Phys. Chem. B* **2000**, *104*, 4618–4624.